



Alternative Exon 9-Encoded Relay Domains Affect More than One Communication Pathway in the *Drosophila* Myosin Head

Marieke J. Bloemink¹, Corey M. Dambacher^{2,3,4}, Aileen F. Knowles⁵, Girish C. Melkani^{2,3,4}, Michael A. Geeves^{1*} and Sanford I. Bernstein^{2,3,4*}

¹Department of Biosciences, University of Kent, Canterbury, Kent CT2 7NJ, UK

²Department of Biology, San Diego State University, San Diego, CA 92182-4614, USA

³Molecular Biology Institute, San Diego State University, San Diego, CA 92182-4614, USA

⁴SDSU Heart Institute, San Diego State University, San Diego, CA 92182-4614, USA

⁵Department of Chemistry and Biochemistry, San Diego State University, San Diego, CA, 92182-1030, USA

Received 18 December 2008;
received in revised form
15 April 2009;
accepted 17 April 2009
Available online
22 April 2009

Edited by M. Moody

We investigated the biochemical and biophysical properties of one of the four alternative regions within the *Drosophila* myosin catalytic domain: the relay domain encoded by exon 9. This domain of the myosin head transmits conformational changes in the nucleotide-binding pocket to the converter domain, which is crucial to coupling catalytic activity with mechanical movement of the lever arm. To study the function of this region, we used chimeric myosins (IFI-9b and EMB-9a), which were generated by exchange of the exon 9-encoded domains between the native embryonic body wall (EMB) and indirect flight muscle isoforms (IFI). Kinetic measurements show that exchange of the exon 9-encoded region alters the kinetic properties of the myosin S1 head. This is reflected in reduced values for ATP-induced actomyosin dissociation rate constant (K_{1k+2}) and ADP affinity (K_{AD}), measured for the chimeric constructs IFI-9b and EMB-9a, compared to wild-type IFI and EMB values. Homology models indicate that, in addition to affecting the communication pathway between the nucleotide-binding pocket and the converter domain, exchange of the relay domains between IFI and EMB affects the communication pathway between the nucleotide-binding pocket and the actin-binding site in the lower 50-kDa domain (loop 2). These results suggest an important role of the relay domain in the regulation of actomyosin cross-bridge kinetics.

© 2009 Elsevier Ltd. All rights reserved.

Keywords: muscle; myosin; *Drosophila*; kinetics; nucleotide

Introduction

The myosin superfamily consists of at least 24 classes of ATP-dependent motor proteins that interact

with actin filaments and are involved in a large number of physiological processes, such as muscle contraction, phagocytosis, cell motility, and vesicle transport.^{1,2} All myosins appear to undergo the same ATP-driven cycle of interaction of myosin with actin, known as the cross-bridge cycle, yet myosins show a wide variety of different mechanical activities. Class II myosins consist of two heavy chains (MHCs) and two pairs of light chains: the regulatory light chains (RLCs) and essential light chains (ELCs). The C-termini of the myosin heavy chains dimerize as a coiled coil ("myosin tail"), whereas the N-termini form the two myosin "heads" or "motor domains." The most familiar activity of class II myosins is muscle contraction.

The various isoforms of *Drosophila melanogaster* muscle MHC are encoded by a single gene (*Mhc*).³ Alternative RNA splicing produces myosin isoforms

*Corresponding authors. E-mail addresses:

m.a.geeves@kent.ac.uk; sbernst@sciences.sdsu.edu.

Present address: C. M. Dambacher, Department of Chemistry and Skaggs Institute for Chemical Biology, The Scripps Research Institute, 10550 N. Torrey Pines Road, SR207, La Jolla, CA 92037, USA.

Abbreviations used: EMB, embryonic body wall; IFI, indirect flight muscle isoform; MHC, myosin II heavy chain; RLC, regulatory light chain; ELC, essential light chain; IFM, indirect flight muscle; EC, embryonic converter; EDTA, ethylenediaminetetraacetic acid; cATP, caged ATP.

with different tissue specificity and functional properties. Of the 19 exons in *Mhc*, 5 exon sets are alternatively spliced, while exon 18 is either included or excluded. Four of the six alternative exon sets encode portions of the motor domain.⁴ The domains encoded by exon 3 (amino acid residues 69–116) and exon 9 (472–528) are located near the sulfhydryl helix, a part of the myosin head that is thought to transduce the chemical energy provided by ATP hydrolysis into movement. The exon 7 domain (301–335) is near the ATP-binding pocket. The exon 11 region (724–764) is part of the converter domain, providing a bridge between the long relay helix encoded by exon 9 and the ELC. Exon 11 encodes the lowest degree of conservation among the alternative regions (38%), followed by exon 7 (56%), exon 3 (75%), and exon 9 (89%).

Exon 9 encodes one of the variable regions in the myosin head, whose location is indicated in Fig. 1a. This region is also known as the “relay helix–loop–helix domain” or “relay domain” and plays a crucial role in the structural coupling between ATP hydro-

lysis and the recovery stroke in the myosin motor. The mechanism of this coupling has recently been modeled in detail based on two crystal structures of *Dictyostelium* myosin II representing the prepower stroke state and the postpower stroke state.⁵ It was proposed that before ATP hydrolysis can occur, the switch-2 loop closes in a stepwise fashion. Closure of switch-2 is linked to an initial rotation of the converter domain via a seesaw pivoting of the relay helix (step 1), whereas the second phase of converter rotation is coupled to the final closing of switch-2 via the SH1 and SH2 helices and the wedge loop (step 2). This proposed coupling mechanism is consistent with the many available myosin crystal structures.^{6,7}

The *Drosophila* relay domain is encoded by alternative exons 9a, 9b, or 9c.³ Exon 9a encodes the indirect flight muscle isoform (IFI) relay domain, while exon 9b encodes a relay domain found within one of the embryonic body wall (EMB) isoforms.⁸ The amino acid sequences of the two relay domains, encoded by exon 9a (IFI) or exon 9b (EMB), are

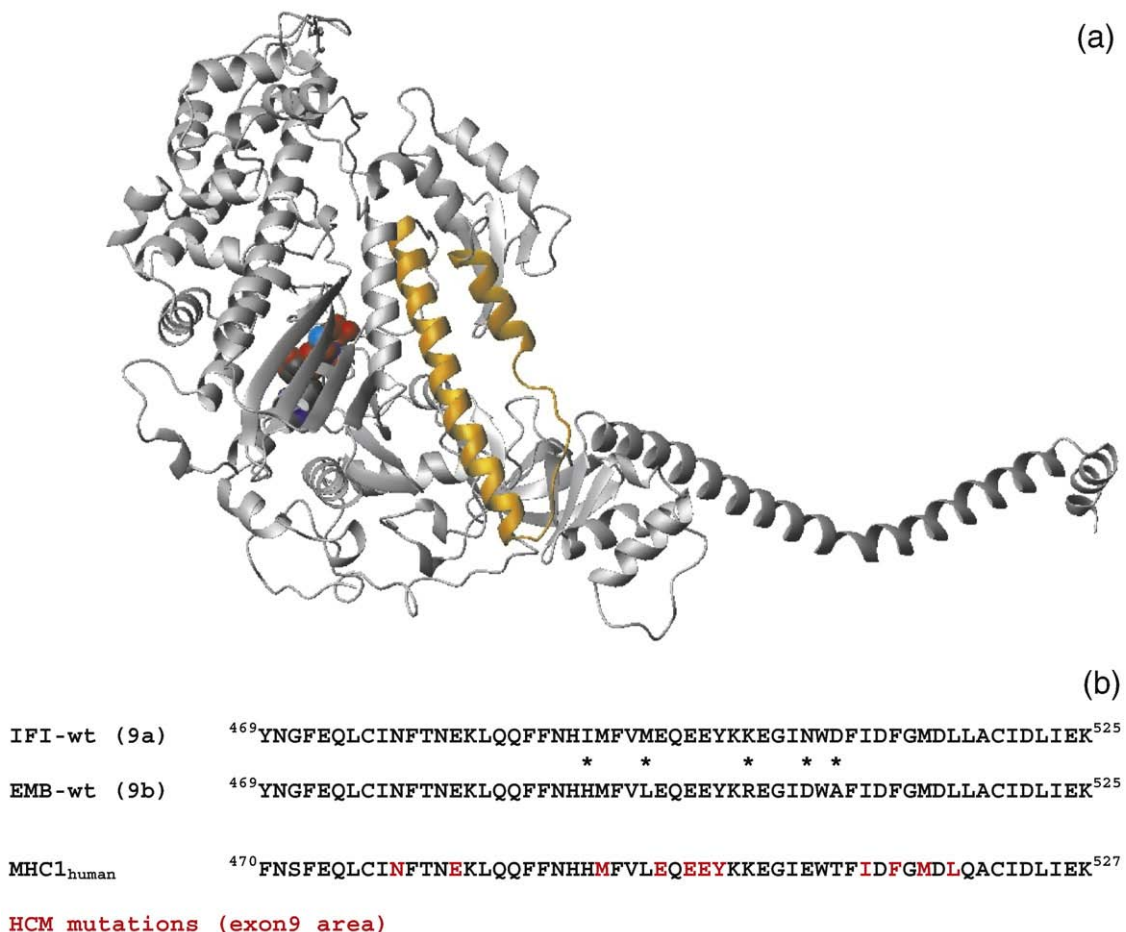


Fig. 1. Location and amino acid sequence of the *Drosophila* exon 9 domain, (a) Homology model of *Drosophila* myosin S1, built using the crystal structure of scallop myosin (postpower stroke conformation) as a template (ExPDB 1kk8). The exon 9 region of *Drosophila* is indicated in yellow (residues 472–528), consisting of the long relay helix P, a loop region and a short helix Q. The location of the nucleotide (space-filling model) is also shown. (b) Primary sequences encoded by exon 9a (IFI) and exon 9b (EMB). The asterisks indicate the five variable residues between the exon 9a and 9b regions. The sequence of the human beta-cardiac MHC is given below (MHC1), with mutations known to cause hypertrophic cardiomyopathy shown in red.

depicted in Fig. 1b and correspond to residues 472–528 of chicken myosin II (or residues 469–525, using *Drosophila* numbering). For reference purposes, we use the chicken numbering throughout this article. We previously generated chimeric myosins (IFI-9b and EMB-9a) by exchanging relay domains between the two native isoforms.⁹ This allows for characterization of functional differences ascribed to alternative versions of this domain. Interchanging the two versions of exon 9 resulted in different effects on the indirect flight muscle (IFM) ultrastructure and performance. IFI-9b flies displayed wild-type structure and stability of IFM myofibrils, while EMB-9a flies showed a significant disruption of muscle structure and myofibril stability when compared to EMB flies. Flight and jump ability tests of flies expressing the IFI-9b myosin isoform were near wild type, while flies expressing the EMB-9a isoform failed to rescue the flightless phenotype and impaired jumping phenotypes observed in flies expressing the EMB isoform. Results from biochemical and mechanical experiments performed on full-length IFI-9b myosin molecules showed that its basal and actin-stimulated ATPase activities, as well as its *in vitro* actin sliding velocity, are similar to those of IFI.⁹ In contrast, the EMB-9a myosin isoform shows a reduction of both basal and actin-stimulated ATPase activities compared to EMB, a marked increase in actin affinity, and lacks the ability to translocate actin filaments *in vitro*.⁹

This article describes steady-state and transient kinetics measurements using S1 fragments of the previously generated exon 9 (IFI-9b and EMB-9a) chimeric MHC isoforms to investigate the roles of the alternative relay domains in regulating the actomyosin cross-bridge cycle. Our results show that several kinetic parameters are affected, including ADP affinity, actin affinity, and ATP-induced actomyosin dissociation. These results indicate that the relay domain, encoded by exon 9, affects more than one signal transduction pathway in the *Drosophila* myosin head. In addition to the expected effects on the communication pathway between the nucleotide-binding pocket and the converter domain, the signal transfer from the nucleotide-binding pocket toward the actin-binding site is altered when relay domains between IFI and EMB are exchanged. Homology models of the chimeric myosin S1 molecules suggest a possible mechanism by which exchanging the relay domain can alter the kinetic properties of the myosin head.

Results

Actin-activated Mg^{2+} -ATPase of the S1 fragments of IFI, EMB, IFI-9b, and EMB-9a

A summary of the steady-state properties of the S1 fragments of wild-type and chimeric myosins is shown in Table 1. This represents the first determination of these kinetic parameters for *Drosophila* myosin S1 ATPase. In agreement with our previous data for full-length wild-type myosins,^{9,10} basal Mg^{2+} -ATPase and actin-activated ATPase values (V_{max}) were significantly higher for IFI S1 (0.074 ± 0.016 and 2.47 ± 0.29 s⁻¹, respectively) compared to EMB S1 (0.016 ± 0.002 and 0.67 ± 0.06 s⁻¹, respectively). There was also a significant difference between K_m values for actin, with EMB S1 showing a twofold increase in actin affinity compared to IFI S1 ($K_m = 2.54 \pm 0.46$ and 5.38 ± 1.13 μ M, respectively). For the chimeric myosins, we found that the steady-state kinetic properties of EMB-9a S1 did not differ significantly from those of EMB S1 (Table 1). For IFI-9b S1, however, we found a small but statistically significant difference in V_{max} compared to IFI S1 ($V_{max} = 3.05 \pm 0.37$ s⁻¹ for IFI-9b and 2.47 ± 0.29 s⁻¹ for IFI). Overall, the basal Mg^{2+} -ATPase activities of the S1 fragments were twofold lower compared to the activities for full-length myosins.⁹ We assessed whether the twofold decrease in basal Mg^{2+} -ATPase activity seen for S1 compared to full-length myosin results from the absence of salt in the S1 assay buffer, but found that eliminating KCl had no appreciable effect on basal Mg^{2+} -ATPase activity of full-length EMB or IFI (data not shown). The V_{max} values of the S1 fragments are approximately twofold higher than those of the full-length myosins (except for EMB). Furthermore, the K_m values of all four S1 fragments are approximately 10- to 60-fold greater than those obtained with the full-length myosins, indicating a significantly weaker apparent affinity for actin for the S1 fragments (Table 1 and Fig. 2).

Determination of the ADP release rate of S1 (k_D) using coumarin-labeled ADP

To estimate the rate constant of ADP dissociation from S1 in the absence of actin, the change in fluorescence of a coumarin-labeled ADP analog [3'-O-{N-[2-(7-diethylaminocoumarin-3-carboxamido)-

Table 1. Steady-state kinetic parameters measured for the IFI, EMB, and exon 9 chimeric S1 isoforms

	IFI S1 (n=5)	EMB S1 (n=3)	IFI-9b S1 (n=5)	EMB-9a S1 (n=6)
Basal Mg^{2+} -ATPase (s ⁻¹)	0.074 ± 0.016^a	0.016 ± 0.002^b	0.077 ± 0.015^a	0.016 ± 0.006^b
Actin-activated ATPase V_{max} (s ⁻¹)	2.47 ± 0.29^a	0.67 ± 0.06^b	$3.05 \pm 0.37^{a,b}$	1.00 ± 0.50^b
K_m (actin) (μ M)	5.38 ± 1.13^a	2.54 ± 0.46^b	4.59 ± 1.45	6.29 ± 3.27

Values are mean \pm SD based on a minimum of three preparations.

^a $p < 0.05$ determined by Student's *t* test compared to EMB.

^b $p < 0.05$ determined by Student's *t* test compared to IFI.

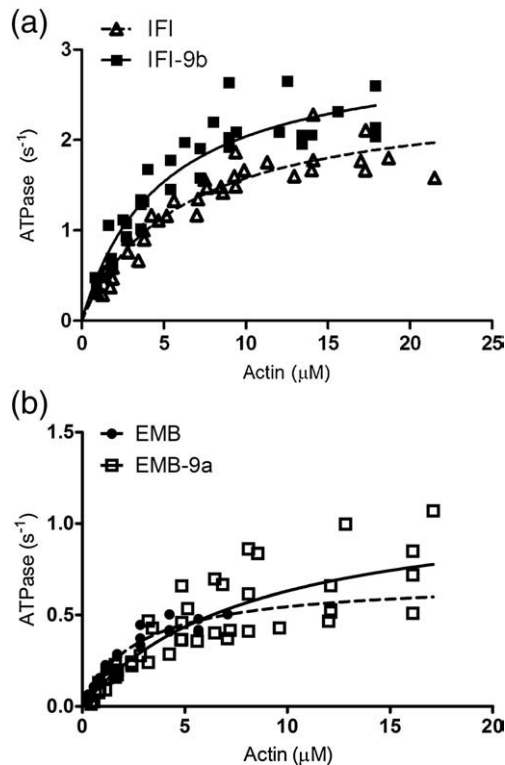


Fig. 2. Actin-activated ATPase activity of IFI, IFI-9b, EMB, and EMB-9a S1. Basal Mg²⁺-ATPase values were subtracted from actin-activated ATPase data and data points were fit to the Michaelis-Menten equation. (a) Actin-activated ATPase activities of IFI S1 (continuous line) and IFI-9b S1 (dashed line) show similar V_{\max} values (2.47 ± 0.29 s⁻¹ for IFI compared to 3.05 ± 0.37 s⁻¹ for IFI-9b) and K_m for actin (5.38 ± 1.13 μM for IFI compared to 4.59 ± 1.45 μM for IFI-9b). (b) Actin-activated ATPase activities of EMB S1 (dashed line, extrapolated beyond data points) and EMB-9a S1 (continuous line) show that their V_{\max} values are similar (0.67 ± 0.06 and 1.00 ± 0.50 s⁻¹, respectively) and that there is no statistical difference between their K_m values (2.54 ± 0.46 and 6.29 ± 3.27 μM, respectively).

ethyl]-carbamoyl ADP, abbreviated to deac-eda ADP] was measured upon its displacement by ATP binding to S1.¹¹ Previously it was shown that this coumarin-labeled analog has very similar kinetic properties compared to ADP. When deac-eda ADP was used, the ADP release rate (k_D) was unchanged for rabbit fast-skeletal myosin S1, the *Dictyostelium* myosin head fragment (M765-1R), and rat EDL myosin S1.¹¹ A single laser flash released 15–20 μM ATP from 100 μM cATP (caged ATP); the fluorescence change resulting from ATP-induced displacement of 1.5 μM deac-eda ADP release is depicted in Fig. 3 for IFI-9b and EMB-9a myosin S1. The measured fluorescence signal could be fitted to a single exponential, from which the resulting k_{obs} gives the ADP release rate (k_D). A $k_D = 2.0 \pm 0.4$ s⁻¹ for IFI-9b and $k_D = 6.0 \pm 0.5$ s⁻¹ for EMB-9a were obtained. The k_D rate of IFI-9b is similar to that of EMB, whereas EMB-9a has a k_D value close to that of IFI¹² (see Table 2). Control measurements using

wild-type myosin S1 (IFI and EMB) confirmed the k_D values reported previously for IFI and EMB. Since the exon 9-encoded region in the myosin head is not very close to the nucleotide-binding pocket (Fig. 1), the large change in k_D rates for IFI-9b and EMB-9a was quite surprising and indicates a critical role for the relay domain in attenuating the rate of ADP release from S1.

Determination of the ATP-induced dissociation of acto-S1 ($K_1 k_{+2}$)

The ATP-induced dissociation of the acto-S1 complex was measured as described previously¹³ using the flash photolysis method. After actin and S1

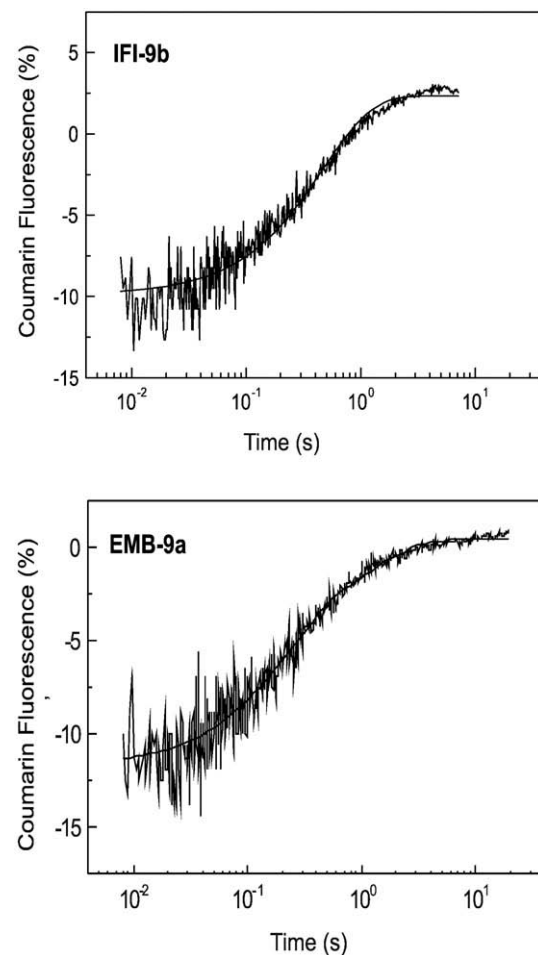


Fig. 3. Rate of deac-eda ADP dissociation (k_D) from *Drosophila* S1 isoforms. The rate constant for ADP dissociation (k_D) from S1 in the absence of actin was determined. Release of ATP (15 μM) from cATP (100 μM) by a single laser flash displaced the deac-eda ADP (1.5 μM) bound to S1 (4 μM). The change in deac-eda ADP fluorescence upon release from S1 was measured and fit with a single exponential to determine k_D . Exchange of either the exon 9a or 9b domain resulted in a modulation of the deac-eda ADP release rate (see Table 2). The dissociation rate of EMB-9a (k_D 6.0 s⁻¹) is faster than that of EMB (k_D 1.8 s⁻¹), while that of IFI-9b (k_D 2.0 s⁻¹) is slower than that of IFI (k_D 7.5 s⁻¹).

Table 2. Transient kinetic parameters measured for the exon 9 chimeric S1 isoforms

	IFI ^a	EMB ^a	IFI-9b	EMB-9a
K_1k_{+2} ($\mu\text{M}^{-1}\text{s}^{-1}$)	0.75 ± 0.08^b	0.91 ± 0.13^c	$0.40 \pm 0.03^{b,c}$	0.52 ± 0.03^b
K_{AD} (μM)	409 ± 26^b	587 ± 48^c	$155 \pm 6^{b,c}$	419 ± 19^b
k_{AD} (s^{-1}) ^d	4090	5870	1550	4190
k_D (s^{-1})	7.5 ± 1.3^b	1.8 ± 0.3^c	2.0 ± 0.4^c	$6.0 \pm 0.5^{b,c}$
K_D (μM) ^e	7.5	1.8	2.0	6.0
K_{AD}/K_D	54.5	326	77.5	69.8
k_{cat} (s^{-1})	0.170 ± 0.006^b	0.028 ± 0.006^c	0.163 ± 0.007^b	$0.097 \pm 0.002^{b,c}$

Values are mean \pm SD based on a minimum of three preparations. K_1k is the second-order rate constant for ATP-induced dissociation of acto-S1. K_D and K_{AD} are dissociation equilibrium constants determined by division of the dissociation rate constant by the association rate constant (e.g., $K_3 = k_{-3}/k_{+3}$). k_D and k_{AD} are the ADP dissociation rate constants in the absence and presence of actin, respectively. K_{AD}/K_D is the thermodynamic coupling constant describing the relationship between actin and ADP affinities. k_{cat} is the catalytic activity.

^a Data are from Ref. 12, except k_{cat} .

^b $p < 0.05$ determined by Student's t test as compared to EMB.

^c $p < 0.05$ determined by Student's t test as compared to IFI.

^d Data are estimated from K_{AD} , assuming an association rate constant of $10^7 \text{ M}^{-1} \text{ s}^{-1}$.

^e Data are estimated from k_D , assuming an association rate constant of $10^6 \text{ M}^{-1} \text{ s}^{-1}$.

were mixed, the sample was subjected to a series of laser flashes with variable intensities releasing different amounts of ATP from cATP. The changes in light scattering (Fig. 4a and b) could be fitted to a single exponential. Plotting the observed rate constant k_{obs} versus ATP concentration allows the apparent second-order rate constant K_1k_{+2} to be determined from the slope of the graph. The results for the two exon 9 chimeras together with the IFI and EMB wild-type S1 are depicted in Fig. 4c. For IFI-9b and EMB-9a, the K_1k_{+2} value is reduced about twofold ($K_1k_{+2} = 0.40 \pm 0.03$ and $0.52 \pm 0.03 \mu\text{M}^{-1} \text{ s}^{-1}$, respectively) compared to wild-type IFI ($K_1k_{+2} = 0.75 \pm 0.08 \mu\text{M}^{-1} \text{ s}^{-1}$) and wild-type EMB ($K_1k_{+2} = 0.91 \pm 0.13 \mu\text{M}^{-1} \text{ s}^{-1}$) (Table 2).

Determination of the ADP affinity of acto-S1 (K_{AD})

The ADP affinity for S1 in the presence of actin, described by the equilibrium dissociation constant K_{AD} , was determined using established methods.¹² The ATP-induced dissociation of acto-S1 was measured in the presence of increasing amounts of ADP. Plotting k_{obs} versus ADP concentration allows K_{AD} to be determined. The measured values of K_{AD} for IFI-9b and EMB-9a are reduced compared to the wild-type values (see Fig. 5 and Table 2). The K_{AD} of IFI-9b ($155 \mu\text{M}$) is more than twofold lower compared to that of IFI ($K_{AD} = 409 \mu\text{M}$), whereas the K_{AD} value for EMB-9a was reduced to $419 \mu\text{M}$, compared to $587 \mu\text{M}$ measured previously for EMB. Thus, exchange of the exon 9-encoded region between IFI and EMB increases the ADP affinity of acto-S1 for both chimeras.

Actin-S1 dissociation by ATP and subsequent reassociation: k_{cat}

S1 ($1 \mu\text{M}$) and actin ($1 \mu\text{M}$) were incubated with cATP. After release of ATP by a single laser flash, the light-scattering signal (resulting from the dissociation reaction) could be fitted to a single exponential

(k_{obs}). Analysis of the complete reaction profile including reassociation gives information on the rate of the ATP-induced dissociation and the time taken to hydrolyze all the released ATP.¹³ Figure 6 shows that the k_{cat} values for IFI-9b and EMB-9a were 0.163 and 0.097 s^{-1} , respectively. The k_{cat} for EMB (0.028 s^{-1}) is lower than the value reported previously for fast vertebrate skeletal muscle S1, using the same experimental setup (0.11 s^{-1}), whereas the k_{cat} for IFI is higher (0.170 s^{-1}).¹³ For IFI-9b, the measured value for k_{cat} (0.163 s^{-1}) is not statistically different from that of IFI. The k_{cat} for EMB-9a (0.097 s^{-1}) is significantly higher compared to that for EMB (Fig. 6 and Table 2).

Homology models: general description of the exon 9 area

Homology models of the two wild-type myosin S1 isoforms (IFI and EMB) and the two chimeras (IFI-9b and EMB-9a) were built in order to understand the results described above at the molecular level. The various states of the myosin head during the cross-bridge cycle are represented by several crystal structures of scallop myosin, and these were chosen as templates to generate three-dimensional (3D) homology models of the IFI and EMB and the chimeras. In the exon 9-encoded area, the rmsd of the myosin backbone between IFI and EMB was $< 0.07 \text{ \AA}$ and followed the same topology for both isoforms. For descriptive purposes, we use the same nomenclature for secondary-structure elements as described previously.¹⁴ As depicted in Fig. 7a, a long helix (helix P, residues 475–505) at the N-terminus of the exon 9 region is followed by a loop (506–516) and then a short helix (helix Q, 517–527). The long helix P contains three residues that are variable between exon 9a and exon 9b, residue 494, which is in the middle of this long helix and can be Ile (exon 9a) or His (exon 9b), residue 498, which is positioned one helix turn further from residue 494 (thus is on the same side

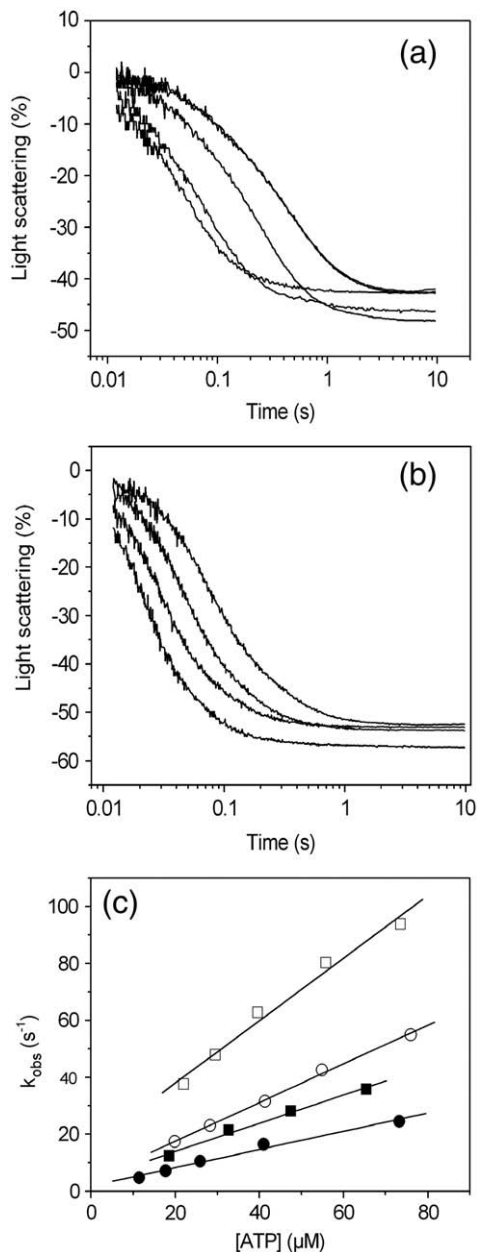


Fig. 4. Kinetic determination of the ATP-induced dissociation rate (K_1k_{+2}) of the S1 isoforms from actin. Light-scattering transients monitoring dissociation of the acto-S1 complex of IFI-9b (a) and EMB-9a (b) after release of various ATP concentrations. Each transient was fitted to a single exponential in order to determine the corresponding k_{obs} . (c) The second-order rate constant (K_1k_{+2}) for the dissociation of S1 from actin is determined from a linear fit to the plot of the k_{obs} versus [ATP]. The linear fits yielded values of $0.40 \pm 0.03 \mu\text{M}^{-1} \text{s}^{-1}$ for IFI-9b (●) compared to $0.75 \pm 0.08 \mu\text{M}^{-1} \text{s}^{-1}$ for IFI (○), and mean values of $0.52 \pm 0.03 \mu\text{M}^{-1} \text{s}^{-1}$ for EMB-9a (■) compared to $0.91 \pm 0.13 \mu\text{M}^{-1} \text{s}^{-1}$ for EMB S1 (□).

of the helix as residue 494), can be Met or Leu, and residue 505, located at the C-terminus of helix P, can be Lys or Arg. The loop between helix P and Q contains the other variable residues (Asn/Asp509 and Asp/Ala511). The short helix Q at

the C-terminal end of exon 9 is identical in the two isoforms.

Exon 9 area: highly conserved interactions

Sequence alignments show that the exon 9-encoded region is a highly conserved area of the myosin head (Fig. 7B). About 50% of the residues in helix P (residue 475–505) are totally conserved, whereas the residues in the loop and helix Q are more variable. Analysis of many myosin crystal structures^{7,15} and modeling work by Fisher *et al.*⁵ have indicated that the relay domain plays a crucial role in the structural coupling between ATP hydrolysis and the recovery stroke in the myosin motor. Closure of switch-2, located in the nucleotide-binding pocket, is linked to an initial rotation of the converter domain via a seesaw pivoting of the relay helix.⁵ Subsequently, the second phase of converter rotation is coupled to the final closing of switch-2 via the SH1 and SH2 helices (residues 691–716) and the wedge loop (His583-Ile584-Ala585).

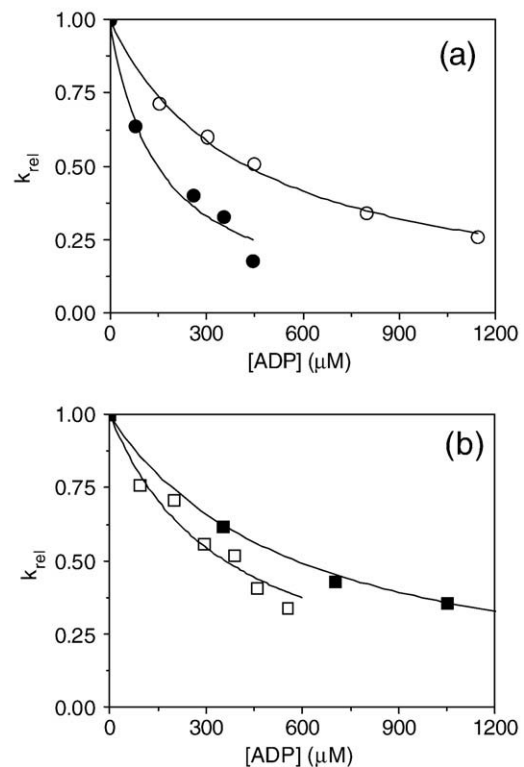


Fig. 5. The affinity of ADP (K_{AD}) for acto-S1. The dissociation of 1 μM acto-S1 was induced by ATP as described for Fig. 4 in the presence of ADP (0–1200 μM). The light-scattering traces were fitted with single exponentials to determine the k_{obs} (not shown). Hyperbolic plots of the k_{obs} versus ADP concentration were fitted with an equation derived from Scheme 1 [$k_{obs} = K_1k_{+2}([ATP]) / (1 + [ADP]/K_{AD})$] to determine K_{AD} . Shown are the relative k_{obs} (k_{rel}) versus ADP concentration plots for easier comparison. (a) For IFI-9b, the fits yielded a value of $155 \pm 6 \mu\text{M}$ for IFI-9b (●) compared to $409 \pm 26 \mu\text{M}$ for IFI (○). (b) For EMB-9a, the fits yielded values of $419 \pm 19 \mu\text{M}$ for EMB-9a (■) compared to $587 \pm 48 \mu\text{M}$ for EMB S1 (□).

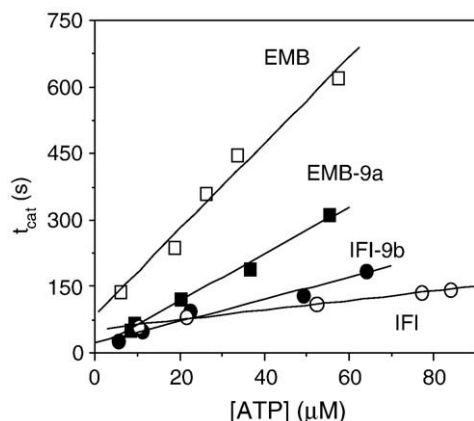


Fig. 6. The turnover number (k_{cat}) for acto-S1. Light-scattering transients monitoring dissociation of the acto-S1 complex and subsequent reassociation were measured using varying amounts of ATP. The time taken to hydrolyze all of the ATP (t_{cat}) was estimated from the time at which the dissociation reaction was 50% complete (t_{diss}) to the time for 50% recovery of light scattering (t_{ass}). This time period (t_{cat}) was linearly dependent on the amount of released ATP as shown here. The steady-state rate of ATP hydrolysis can be determined from the inverse of the slope (steady-state rate = $[\text{ATP}]/t_{\text{cat}}$), allowing one to determine the catalytic activity (k_{cat}). The catalytic activity of IFI-9b ($k_{\text{cat}} = 0.163 \text{ s}^{-1}$) (●) is not different compared to IFI (0.170 s^{-1}) (○), whereas k_{cat} of EMB-9a (0.097 s^{-1}) (■) has increased compared to EMB (0.028 s^{-1}) (□).

Our homology models show that *Drosophila* myosin residues Gln477, Asn481, and Asn484, all located at the N-terminus of helix P, form hydrogen bonds with switch-2 residues Glu468, Ala465, and Gly466 (not shown). The contacts between switch-2 and the N-terminal part of helix P are maintained throughout the cross-bridge cycle, since they can be seen in all homology models that were built using different scallop structures as templates. These contacts allow the relay helix to follow the movements of switch-2 in a seesaw-like fashion, in accordance with the model of Fischer *et al.* for *Dictyostelium* myosin II.¹⁶ The highly conserved residues Phe490 and Phe491 form the fulcrum point, anchoring the relay helix P to the third strand of the central β -sheet via residue Phe673, also in agreement with the Fisher model for *Dictyostelium* myosin II. The second stage of converter rotation, coupled to the final closing of switch-2 via the SH helices and the wedge loop, involves other highly conserved exon 9 region residues. Contacts with the wedge loop involve exon 9 region residues Glu485, Gln488, and Cys522, whereas contacts toward the SH1 and SH2 helices involve the conserved residues Gln488, Asn492, Glu499, Glu502, Tyr503, Asp514, and Asp518. None of the five variable residues encoded by exon 9a/b is involved in direct contacts with either switch-2, the wedge loop or the SH1 and SH2 relay helices, indicating these switch interactions are a conserved feature of both isoforms.

Exon 9 area: nonconserved interactions

Inspection of the exon 9-encoded domain in the homology models reveals close interactions between this domain and the region encoded by alternative exon 11, a variable portion of the myosin head of *Drosophila* that is located in the converter domain. These interactions are summarized in Fig. 8. Comparison of IFI and EMB shows that certain contacts between the relay domain and the converter domain are conserved for both isoforms, such as salt bridges from Glu502 toward Lys764 and Glu506 toward Lys764 and Thr763. However, the two variable residues 509 and 511 are also involved in contacts toward the converter domain. For IFI, the side chains of Asn509 and Asp511 make contacts toward the side chain of residue Arg759, whereas EMB only has Asp509 that can form a salt bridge toward Arg759 (since EMB residue 511 is an Ala). One variable residue encoded by exon 11 (Asn762) is also involved in contacts with the EMB exon 9 region, whereas this contact is missing for IFI. Figure 8 also shows that the interactions between the relay area (encoded by exon 9) and the converter domain (encoded by exon 11) not only depend on the particular myosin isoform but also on the conformational state of the myosin head. The two variable residues 509 and 511 are not always in contact with residue Arg759 in the converter domain. For instance, contacts between Asp511 and Arg759 are seen only for IFI in the postpower stroke conformation, suggesting their formation and breaking are part of the cross-bridge cycle (Fig. S1). Homology models of EMB-9a show that this chimeric molecule is able to form a salt bridge between Arg759 and Asp511 in the near-rigor state (Fig. 8). This interaction is not seen for EMB, which has Ala511, and this additional contact may contribute to the lack of motility observed for the chimeric EMB-9a isoform (see Discussion).

Residue 505, either an Arg or Lys, is located at the C-terminus of the relay helix. This residue is involved in an intrahelical salt bridge toward Glu501 and Glu502 (Fig. 9) when myosin is in the prepower stroke state, that is, when ExPDB 1qvi is used as template to build the model. For the other three states, this intrahelical salt bridge is absent, suggesting its formation and deformation are part of the cross-bridge cycle. Intrahelical salt bridges are a stabilizing factor of monomeric α -helices and can vary in strength. Because Arg is able to form two charged hydrogen bonds to the carboxyl group of Glu, whereas Lys can form only one, thermophilic enzymes prefer Arg residues over Lys in order to enhance the stability of the protein.¹⁷ This may be the reason that the slower isoform EMB has Arg in its intrahelical salt bridge, whereas the faster IFI isoform is using Lys. Looking at the alignments of various myosins (Fig. 7b), it appears that, except for EMB, the fast IFI and all other skeletal myosin II isoforms have a Lys at this position. The slow EMB is more akin to the slower myosin forms, such as smooth myosins and *Dictyostelium* myosin IE, which

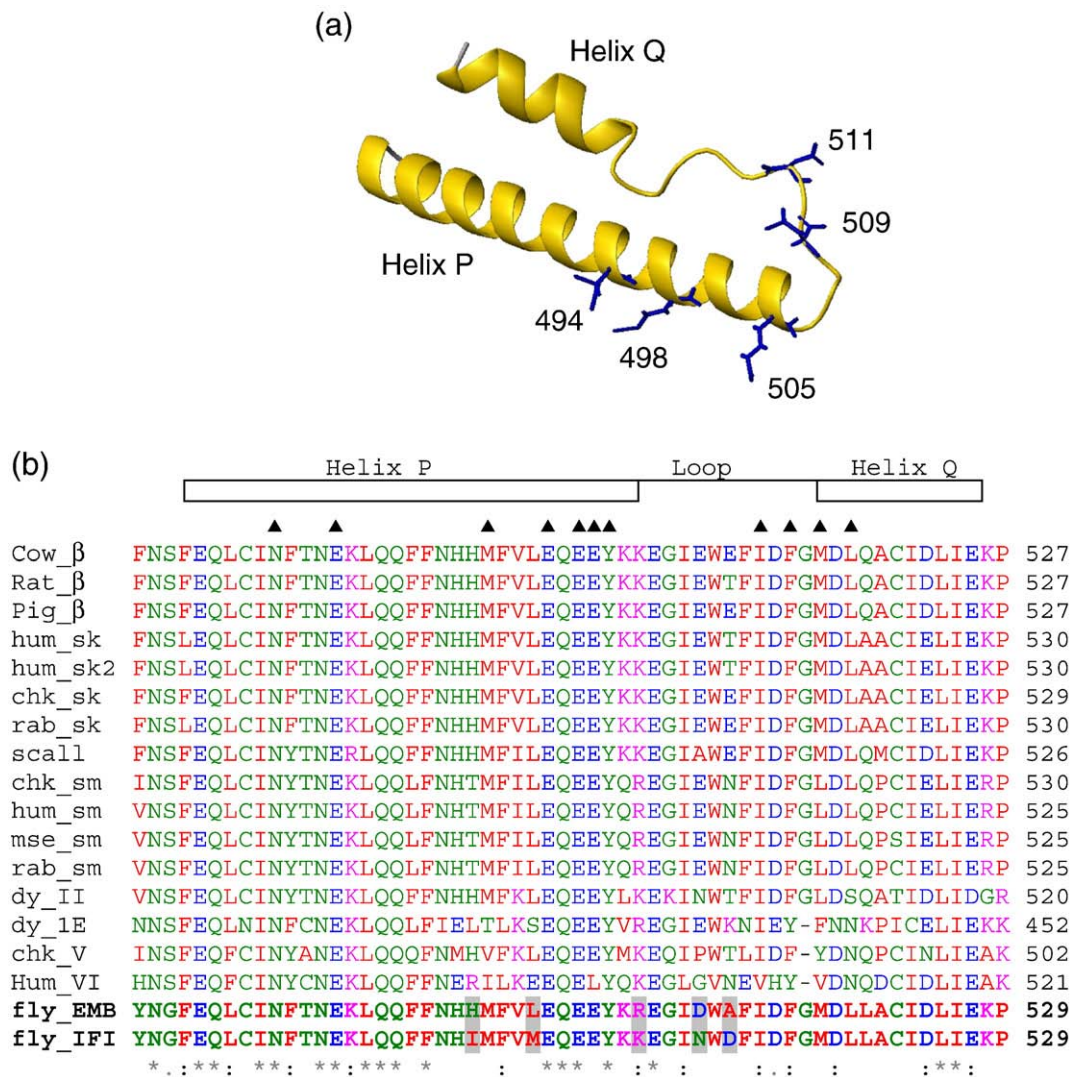


Fig. 7. Primary and secondary structure of the exon 9-encoded region in the myosin head. (a) The secondary structure of the exon 9-encoded region is shown with helix P (containing three variable residues), a loop region with two variable residues, and helix Q. The side chains of the residues that vary between exon 9a and 9b regions are indicated (the IFI form is depicted). (b) Sequence alignment of various myosins showing exon 9-encoded regions with shaded residues indicating the 5 variable residues between IFI and EMB. “*” indicates that the residues are identical in all sequences in the alignment. “:” represents conserved substitutions, whereas “.” indicates semiconserved substitutions. The corresponding human β-myosin cardiomyopathy sites in the exon 9-encoded domains are indicated with a ▲.

all have an Arg instead. The Glu501 residue is completely conserved; indicating this intrahelical salt bridge in the myosin relay helix is a universal feature.

Residue 494, which can be either Ile or His, is located about halfway along the relay helix (Fig. 7a). The position of this residue is of interest because it is next to Met495, the residue postulated to be involved in the local unwinding of the relay helix during the cross-bridge cycle.¹⁶ Residue 494 is also close to the fulcrum point (Phe490, Phe491, and Phe673), which anchors the relay helix to the third strand of the central β-sheet, and its presence may reinforce the anchoring point. Inspection of the homology models (Fig. 10) shows that EMB residue His494¹⁴ is able to make a hydrogen bond from the imidazole ring (H donor) toward the carbonyl of residue Leu666. This residue is located at the C-

terminus of helix W and 100% conserved. Helix W is located immediately after loop 2, also known as the actin-binding loop, and may be part of the communication pathway between the relay domain (encoded by exon 9) and the actin-binding site in the lower 50-kDa domain of the myosin head (see Fig. 10, Fig. S2, and Discussion). IFI has an Ile residue at position 494 and is not able to make this contact toward helix W.

Discussion

In this study, we utilized S1 fragments of wild-type (IFI and EMB) and chimeric (IFI-9b and EMB-9a) myosins to continue our analysis of the contribution of alternative exons encoding the *Drosophila* myosin head to myosin isoform functional differences. This

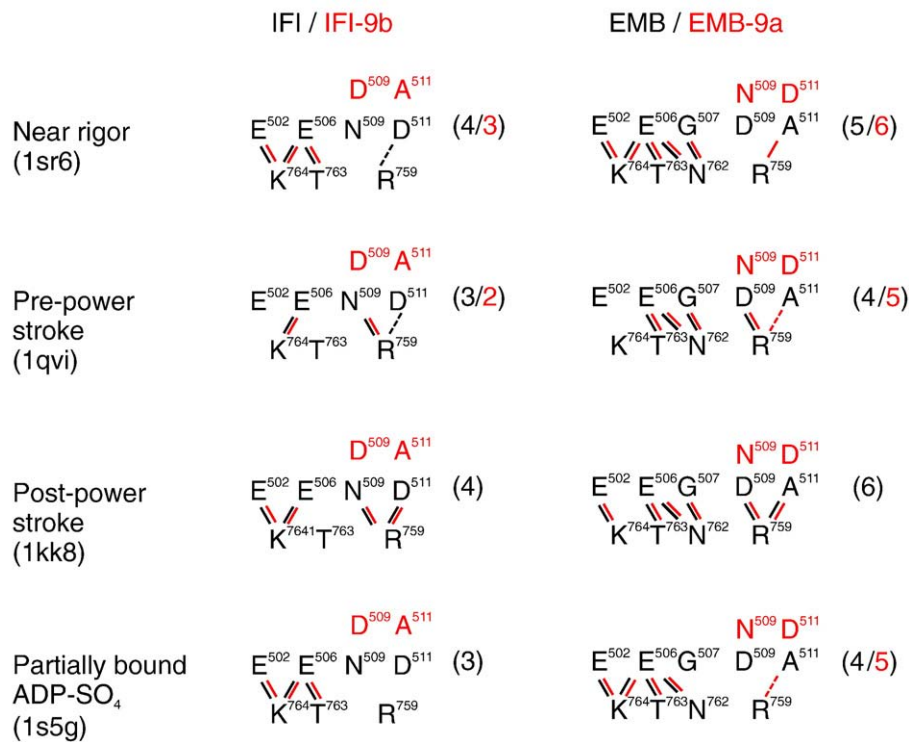


Fig. 8. Interaction of the exon 9-encoded domain with the converter region. Summary of the contact points between the relay area (encoded by exon 9) and the converter domain (encoded by exon 11) for the wild-type and chimeric constructs using homology models. Black is used for the wild-type and red for the chimeric constructs. Short thick lines represent close contacts (within 1.8–4.5 Å), whereas dashed lines indicate weaker contacts (within 4.5–5 Å). The total number of contacts between the two variable domains is indicated for each conformation. Note the extra contact for EMB-9a between residue 511 and Arg759 in the near-rigor states, which may be responsible for the lack of *in vitro* actin motility observed for this mutant.

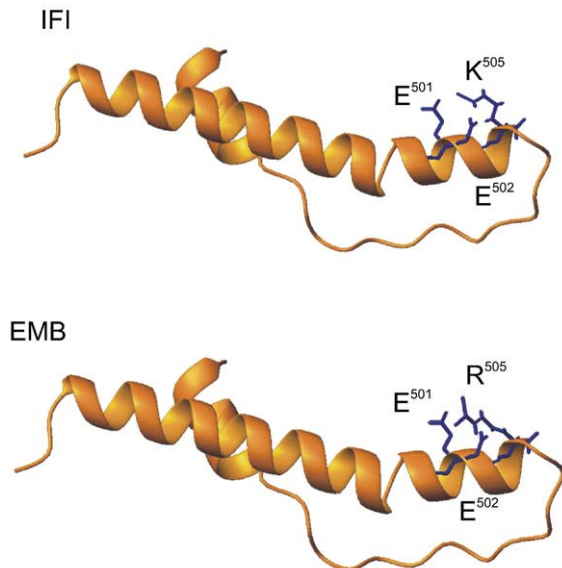


Fig. 9. An intrahelical salt bridge stabilizes the pre-power stroke conformation. Comparison of exon 9a and exon 9b encoded regions in the prepower stroke state shows the presence of an intrahelical salt bridge, involving residues Glu501, Glu502, and residue 505, which can be either Arg (EMB) or Lys (IFI). This salt bridge is not present in any of the other states (1sr6, 1kk8, 1s5g), indicating its formation and deformation are part of the cross-bridge cycle.

study focused on the structure and function of alternative relay domains encoded by exon 9. We determined the steady-state kinetic parameters of the actin-activated ATPase activities and examined the transient kinetics of the cross-bridge cycle for each of these molecules. Transient kinetics data showed significant changes due to relay domain switching. Homology modeling allowed us to predict how isoform-specific amino acid residues affect the structural and functional properties of the chimeric molecules. Our studies indicate that the relay domain serves a central role in communicating between the nucleotide-binding pocket and both the converter domain and the actin-binding site.

Ours are the first reported steady-state ATPase data for *Drosophila* myosin S1. The data show that basal ATPase rates are much higher for the IFI S1 than for EMB S1. This is similar to the actin-activated ATPase where both the V_{max} and K_m values were about fourfold higher for IFI S1 compared to EMB S1. The switching of exons 9a and 9b made no dramatic difference to the values for either basal or actin-activated ATPases, indicating that the rate-limiting step does not change after exons 9a and 9b are switched. Note that the values for EMB-9a S1 were quite variable compared to EMB S1 values, necessitating the preparation of numerous samples. This may be related to the early myofibril defects

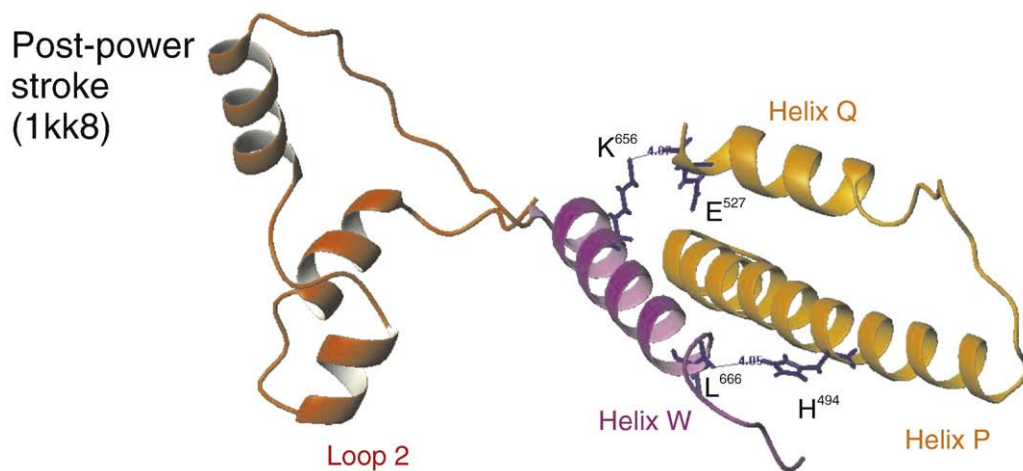


Fig. 10. Helix W is part of the signaling pathway between the exon 9-encoded region and the actin-binding loop 2 in the lower 50-kDa domain. In the prepower stroke state (1qvi), exon 9-encoded residue Glu527 (helix Q) interacts with helix W residues Asn660 and residue Lys656, whereas in the postpower stroke state (1kk8, shown here) the interaction between Glu527 and Lys656 remains but the contact between the exon 9 region and Asn660 is lost. In the near-rigor state, the side chain of residue Glu527 is not in contact with helix W but forms a salt bridge with exon 9-encoded residue Lys486. The relay domain in EMB and IFI-9b (encoded by exon 9b) has an additional contact from His491 toward helix W residue Leu666, but this is only seen in the postpower stroke state (1kk8). See [Supplementary Fig. S2](#) for all three states.

seen in the EMB-9a line,⁹ which might affect the stability of myofibrillar proteins. Overall, however, it appears that the steady-state parameters of S1 are not dramatically affected by the relay area switches.

In contrast to that of full-length myosin, measurements of actin-activated ATPase activity of *Drosophila* S1 required the absence of KCl, since actin activation was undetectable in the presence of low (20 mM) KCl concentrations (data not shown). This presumably reflects the relatively low affinity of *Drosophila* S1 for actin in the presence of ATP. Indeed, the K_m for actin of all four *Drosophila* myosin S1 fragments is more than 10 times larger compared to that of full-length myosins. Reduced actin affinity and increased K_m for actin have been reported for S1 of other species and may well reflect the higher affinity of the double-headed myosin for actin.¹⁸ Direct comparison of the S1 and myosin basal ATPase and V_{max} values is difficult because of the different assay conditions, but the relative values are generally comparable. The basal Mg^{2+} -ATPase values for all four *Drosophila* S1 fragments were twofold lower than those of the full-length myosins, and this difference is not attributable to differences in salt concentration (data not shown). The V_{max} values of the IFI S1 isoforms were about twofold higher than those of full-length, while those of the EMB S1 constructs and myosin were similar.

In contrast to the steady-state ATPase results, the transient kinetics data revealed significant alterations in various kinetic properties of the myosin head after exchange of the exon 9-encoded region. Binding of ATP to the myosin head induces conformational changes in the nucleotide-binding pocket involving the highly conserved switch-1 and switch-2 loops. The general consensus is that switch-1 is involved in

the transmission of information between the nucleotide- and actin-binding regions, whereas switch-2 plays a role in communicating changes in the nucleotide-binding pocket to the converter domain via the relay domain encoded by exon 9. Our results indicate that the *Drosophila* myosin relay domain can also influence the communication pathway between the nucleotide-binding pocket and the actin-binding site. Exchange of the relay domain between IFI and EMB results in a twofold reduction of the ATP-induced dissociation rate of acto-S1 (K_{1k+2}) for the two chimeras and alters the affinity of acto-S1 for ADP (smaller K_{AD} value) compared to the wild type. Both results indicate a less efficient communication pathway between the nucleotide-binding pocket and the actin-binding site in the chimeras. ATP-binding induces closure of the nucleotide-binding pocket and subsequent opening of the actin-binding cleft, releasing actin from myosin. This process is slower after exchange of the exon 9-encoded domain, as is reflected in the reduced K_{1k+2} values of the chimeras. Upon binding of actin to myosin-ADP the actin-binding cleft closes and the nucleotide-binding pocket opens, allowing ADP release. This process is also slower for the chimeras, since their K_{AD} values are reduced, indicating an increase in ADP affinity and slower ADP release.

The ratio K_{AD}/K_D (Table 2) is termed the thermodynamic coupling constant, and this parameter describes the effect of actin on ADP affinity of myosin (K_{AD}/K_D). A strong coupling constant (~ 50) is found in fast myosins, indicating that the presence of actin significantly weakens ADP affinity and *vice versa*. The coupling constant for IFI-9b S1 (78) and EMB-9a S1 (70) suggests that these isoforms are more similar to IFI (55) than to EMB (326). For IFI-9b S1, both K_{AD} and K_D parameters are reduced

compared to that of the wild-type IFI, so that the K_{AD}/K_D ratio is similar to that of IFI S1. Exchanging the exon 9a-encoded region in EMB results in a shift of both K_D and K_{AD} toward the IFI S1 values, thus reducing the coupling constant to IFI S1 levels.

The homology modeling indicates that exchange of the region encoded by exon 9 in the myosin head of *Drosophila* between IFI and EMB could affect the communication pathway between the nucleotide-binding pocket and the converter domain. Certain contacts between exon 9 and exon 11 regions are conserved for both isoforms (Fig. 8), in agreement with earlier observations, which showed that the myosin relay domain and the converter domain remain in contact throughout the actomyosin ATPase cycle.¹⁹ However, the homology models suggest that other contacts between the regions encoded by exon 9 and exon 11 are variable between the two isoforms and may be altered, depending on the state of the myosin head (Fig. 8). This is true in particular for the two residues 509 and 511, which are different in IFI and EMB and could serve to fine-tune the kinetic and mechanochemical properties of the myosin head. Exchange of the EMB residues Asp509 and Ala511 for the IFI residues Asn509 and Asp511 may alter the interface between the exon 9 and exon 11 regions and might even be responsible for the lack of motility observed for the EMB-9a mutant.⁹ Introducing additional interactions between the relay and converter domain in the near-rigor conformation for EMB-9a may weaken the formation of the prepower stroke conformation, in particular when using an intrahelical salt bridge that contributes less electrostatic energy to the prepower stroke conformation compared to EMB (using Lys505 *versus* Arg505, respectively). The lack of *in vitro* motility observed with the EMB-9a isoform, however, is overcome in fibers where maximum power generation (P_{max}) and optimal frequency of power generation (f_{max}) increased 2.5-fold and 1.4-fold, respectively, compared to EMB fibers.²⁰ This may be due to an enhanced sensitivity to oscillatory load for the IFI relay domain. The models suggest that replacement of the IFI residues Asn509 and Asp511 with the EMB residues Asp509 and Ala511 results in weaker interactions between the relay and converter domains for IFI-9b compared to IFI. This could be responsible for decreasing P_{max} and f_{max} to 70% and 83%, respectively, of IFI fiber values.²⁰

Exchanging the region encoded by exon 11 between IFI and EMB is also expected to affect the interface between the relay domain and converter domain but should leave the intrahelical salt bridge in helix P unaltered. It was previously reported that exchange of the exon 11-encoded region between IFI and EMB does alter the mechanochemical properties of these chimeric isoforms. IFI-EC [IFI containing the embryonic converter (EC) domain] yielded a decrease in actin sliding velocity ($2.7 \mu\text{m}\cdot\text{s}^{-1}$) compared to IFI ($6.4 \mu\text{m}\cdot\text{s}^{-1}$), whereas EMB-IC (EMB containing the converter domain from the IFI) showed an increase in actin sliding velocity com-

pared to EMB ($5.4 \mu\text{m}\cdot\text{s}^{-1}$ *versus* $0.7 \mu\text{m}\cdot\text{s}^{-1}$, respectively).²¹ Transient kinetic data for these chimeras showed that the embryonic converter domain in an IFI background has a larger effect on the kinetic properties of the myosin head than the IFI converter in the EMB background.¹² Although EMB-IC and IFI-9b chimeras share the same relay and converter domain sequences (encoded by exon 9b and IC), as is also true for IFI-EC and EMB-9a, which share the regions encoded by exon 9a and EC, their mechanochemical properties are not identical. This is likely due to the involvement of the other two variable domains in the myosin head encoded by exons 3 and 7.

However, one kinetic parameter that is identical between EMB-IC and IFI-9b chimeras is the ADP release rate in the absence of actin: k_D . Taking into account previous results¹² where exon 11 is exchanged between IFI and EMB (IFI-EC and EMB-IC), one can summarize the results for k_D as shown in Table 3. From this table, one can conclude that without actin present, the constructs that express exon 9a have fast ADP release rates ($k_D = 6\text{--}8 \text{ s}^{-1}$), and the myosin constructs expressing exon 9b have slow ADP release ($k_D = 1.7\text{--}2 \text{ s}^{-1}$). This is independent of exon 11, suggesting that the effect of exon 9 swapping on k_D is unlikely to be due to the variable exon 9-encoded residues 509 and 511, located at the interface with exon 11. Our hypothesis is that for these *Drosophila* myosins it is exon 9-encoded residue 505 (R/K), involved in the intrahelical salt bridge in the long relay helix P, that is responsible for the k_D rate. All constructs with a R505 display a slow k_D , whereas all constructs with a K505 are considerably faster.

Apart from affecting the communication pathway between the nucleotide-binding pocket and the converter domain, as suggested by the homology models, exchange of exon 9-encoded regions between IFI and EMB also affects the communication pathway from the nucleotide-binding pocket toward the actin-binding site. This is reflected in the reduced values for K_1k_{+2} and K_{AD} , measured for the chimeric constructs IFI-9b and EMB-9a compared to IFI and EMB. The homology models indicate a role for helix W (650–667) in this communication pathway. This helix immediately follows loop 2, which is a well-known actin-binding loop and is located in the lower 50-kDa domain.²² Helix W is also close to

Table 3. Summary of the ADP release rate k_D as a function of chimeric exon 9 and exon 11-expressing isoforms

	Exon 9	Exon 11	k_D (s^{-1})
IFI	9a	11e	7.5
IFI-EC	9a	11c	8.4
EMB-9a	9a	11c	6.0
EMB	9b	11c	1.8
EMB-IC	9b	11e	1.7
IFI-9b	9b	11e	2.0

Values for IFI-EC and EMB-IC are from Miller *et al.*¹²

the N-terminus of the long relay helix P and the C-terminal part of the short helix Q, both of which are part of the region encoded by exon 9 (see Fig. 10 and Fig. S2). In the prepower stroke state, exon 9-encoded residue Glu527 (helix Q) interacts with helix W residues Asn660 and residue Lys656, whereas in the postpower stroke state, the interaction between Glu527 and Lys656 remains but the contact between exon 9-encoded residues and Asn660 is lost. In the near-rigor state, the side chain of residue Glu527 is not in contact with helix W but forms a salt bridge with exon 9-encoded residue Lys486 (Fig. S2). Thus, helix W is in an excellent position to communicate changes from the actin-binding site toward the relay domain and *vice versa*, as was proposed previously for $\alpha 5$, a helix W equivalent in kinesin.²³ The region encoded by exon 9b, present in EMB and IFI-9b, has an additional contact from His494 toward helix W residue Leu666, but this is only seen in the postpower stroke state and is absent in the other three states. Sequence alignments show that residue His494 is variable among the myosins (Fig. 7b). Myosin II and V family members have a His residue, smooth muscle myosins have a Thr, and myosin VI has an Arg residue at this position. Crystal structures of myosin VI showed that this Arg residue (R487) is able to form hydrogen bonds toward helix W residues Ser660, Thr661, and Ala663 in both the nucleotide-free state and in the prepower stroke state (ExPDB 2BKH and 2V26, respectively).^{24,25}

Biological implications

The exon 9 domain in human β -myosin heavy chain contains several sites that, when mutated, result in hypertrophic cardiomyopathy. Mutations have been reported for Asn479/Ser,²⁶ Glu483/Lys,^{26,27} Met493/Leu/Lys,²⁸ Glu497/Asp,²⁹ Glu499/Lys,³⁰ Glu500/Ala,³¹ Tyr501/His/Cys,²⁸ Ile511/Phe,³² Ile511/Thr,³³ Phe513/Cys,³⁴ Met515/Arg,³³ and Leu517/Met³⁵ (the equivalent exon 9-encoded residues in *Drosophila* are indicated in Fig. 7b with \blacktriangle). Based on the homology models, Asn479/Ser is expected to alter the interaction between helix P and switch 2, whereas Glu483/Lys is likely to affect the contacts with the wedge loop. Various cardiomyopathy mutations will influence contacts from the exon 9-encoded domain toward the SH1 and SH2 helices (Glu497/Asp and Tyr501/His/Cys) and toward the converter domain (Glu500/Ala). Mutating the residues involved in the intrahelical salt bridge of helix P also can cause HCM (Glu499/Lys and Glu500/Ala) as can mutating the residue thought to be involved in the local unwinding of helix P (Met493/Leu/Lys). HCM mutations have also been reported for helix W residues Arg652/Gly, Met659/Ile, and Arg663/Ser/Cys/His. Based upon our kinetic measurements and molecular modeling, we propose that these mutations alter myosin function by disrupting the relay pathway between the nucleotide-binding

pocket and the actin-binding site in the lower 50-kDa domain.

Materials and Methods

Generation of subfragment-1 (S1) from isolated full-length myosin

Myosin was isolated from the IFM of 170–250 wild-type or transgenic flies (those expressing the IFI, EMB, EMB-9a, or IFI-9b myosin isoforms in the IFM) as previously described.³⁶ The production of S1 by α -chymotrypsin digestion was carried out using a method based on that of Silva *et al.*³⁷ with the following modifications: The final myosin pellets obtained after centrifugation of a myosin solution in low-salt buffer were dissolved in 20 μ l of high-salt digest buffer [480 mM NaCl, 20 mM Na₂PO₄, pH 7.0, 1 mM ethylenediaminetetraacetic acid (EDTA), and 20 mM DTT]. The myosin solution was then diluted with 60 μ l of salt-free digest buffer (20 mM Na₂PO₄, pH 7.0, 1 mM EDTA, and 20 mM DTT) to reduce the NaCl concentration to 120 mM. The myosin solution was placed at 20 °C for 5 min for temperature equilibration, followed by addition of α -chymotrypsin (0.2 mg/ml) and further incubation for 4.5 min. Phenylmethylsulfonyl fluoride was added to a final concentration of 1.5 mM to quench the reaction. The myosin solution was subsequently centrifuged at 70,000 rpm (TLA 100.3 rotor) for 30 min in a Beckman ultracentrifuge to pellet the undigested myosin and myosin rods. The supernatant containing the S1 was removed and diluted to 1 ml with low-salt buffer (30 mM KCl, 5 mM MgCl₂, 20 mM Mops, pH 7.0, and 4 mM DTT). To concentrate the S1, the samples were centrifuged at 12,000g in a Sorvall MC 12V at 4 °C using a Millipore Ultrafree 0.5 μ m centrifugal filter Biomax-5 with a 5000-kDa cutoff. The final volume of the supernatant was 40–60 μ l. S1 concentration was determined from A_{280} ($=0.75 \text{ cm}^{-1}$ for 1 mg S1 per milliliter) and were in the range of 20–30 μ M. The S1 samples were stored on ice and used within 1 day for steady-state kinetics experiments and within 1 week for transient kinetics experiments.

Actin preparation

G-actin was isolated from acetone powder of chicken skeletal muscle as described previously.³⁸ After one cycle of polymerization–depolymerization, soluble G-actin obtained after dialysis against 2 mM Tris–Cl (pH 8), 0.2 mM ATP, 2 mM CaCl₂, and 1 mM DTT was quantified spectrophotometrically using an extinction coefficient of 0.62 cm^{-1} ($A_{310 \text{ nm}} - A_{290 \text{ nm}}$) for 1 mg actin ml⁻¹. Under standard preparation condition, the concentrations of G-actin solutions obtained were in the range of 30–120 μ M. To obtain a G-actin solution of 200–400 μ M, the G-actin solution was concentrated using the Millipore Biomax-5 filter as described above. F-actin was prepared by adding 1 volume of 10 \times polymerization buffer [50 mM Tris–Cl (pH 8), 0.5 M KCl, 20 mM MgCl₂, and 10 mM ATP] to 9 volumes of G-actin, stored on ice at 4 °C, and used within 1 month of preparation for actin-activated Mg²⁺-ATPase assays. Rabbit skeletal muscle actin was used for transient kinetic experiments and prepared according to established methods.³⁸ Quantification of the purified actin was based on a molecular mass of 42 kDa and an extinction coefficient

of $E^{1\%} = 1.104 \text{ cm}^{-1}$ at 280 nm absorbance. Prior to use, rabbit F-actin was mixed with an equimolar concentration of phalloidin and incubated at 4 °C for at least 4 h in order to stabilize the filaments.

Basal and actin-stimulated Mg^{2+} -ATPase assays

ATPase activities were determined using $[\gamma\text{-}^{32}\text{P}]\text{ATP}$. Actin-activated Mg^{2+} -ATPase using $\sim 2 \mu\text{g}$ S1 was determined as previously described for full-length myosins¹⁰ with modifications. No salt (KCl) was added to the Mg^{2+} -ATPase assay solution (10 mM imidazole, 0.1 mM CaCl_2 , 1 mM MgCl_2 , 1 mM $[\gamma\text{-}^{32}\text{P}]\text{ATP}$), and approximately 10-fold F-actin concentrations were required to obtain near-maximal levels of stimulation as previously reported for assays using full-length myosin. The working F-actin solution had a concentration of $\sim 400 \mu\text{M}$ to minimize the amount of nonradioactive ATP added to the ATPase reaction mixture. Basal Mg^{2+} -ATPase activities obtained in the absence of actin were subtracted from all data points, which were fit with the Michaelis-Menten equation.

Flash photolysis system

Because of the small amounts of protein available, flash photolysis was used to measure the transient kinetics of the *Drosophila* myosin S1 mutants as described previously.^{12,39} Fast skeletal S1 (from rabbit) was used for testing the flash photolysis system on each occasion and just prior to measuring the *Drosophila* myosin constructs of interest. The experiment was identical in all details except fast skeletal S1 replaces the *Drosophila* protein. Thus, all aspects of the experiment, except the *Drosophila* protein, are carefully controlled. The ATP-induced dissociation of the acto-S1 complex was followed by measuring changes in the light-scattering signal, whereas the dissociation of nucleotide from S1 alone was detected by changes in fluorescence using coumarin-labeled ADP⁴⁰ (deac-eda ADP). All light-scattering experiments were conducted in a low-salt buffer (pH 7.0, 30 mM KCl, 5 mM MgCl_2 , 20 mM Mops, and 4 mM DTT) with 1 μM actin, 1–3 μM S1, 500 μM cATP, 10 mM DTT, and either apyrase (2 U/ml) for ATP-induced dissociation of acto-S1 or ADP (various concentrations) and a glucose-hexokinase system (0.03 U/ml hexokinase, 1 mM glucose, and 100 μM Ap_5A [P^1, P^5 -di(adenosine 5')-pentaphosphate]) for determination of K_{AD} . Each sample was subjected to multiple laser flashes in order to release variable amounts of ATP from cATP. During K_{AD} determination, ADP and cATP were added after each flash. The deac-eda ADP dissociation experiments (k_{D}) were also performed in low-salt buffer and contained 4 μM S1, 1.5 μM deac-eda ATP (source of deac-eda ADP), and 100 μM cATP. For the determination of k_{cat} , the acto-S1

sample, incubated without apyrase, was irradiated by a series of laser pulses of different intensities, which released a range of ATP concentrations (10–70 μM). The time taken to hydrolyze all of the ATP (t_{cat}) was estimated from the time at which the dissociation reaction was 50% complete (t_{diss}) to the time for 50% recovery (t_{ass}).¹³ Plotting t_{cat} versus ATP concentration allows one to estimate the steady-state rate of ATP hydrolysis according to Eq. (1):

$$\text{Steady-state rate} = [\text{ATP}]/t_{\text{cat}} \quad (1)$$

from which one can determine the k_{cat} [Eq. (2)]:

$$k_{\text{cat}} = \text{steady-state rate}/[\text{S1}] \quad (2)$$

Analysis of the transient kinetics data

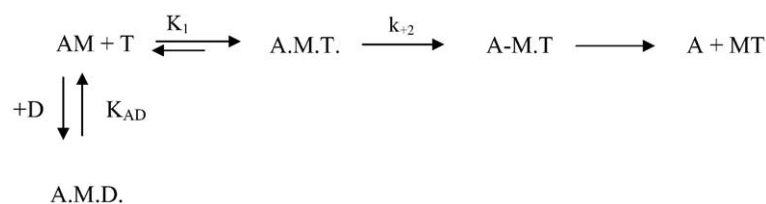
Scheme 1 was used to analyze the transient kinetics data. Equation (3) was derived from the interaction of actin and S1 with ATP and ADP (shown in Scheme 1) and was used to determine K_{AD} .

$$k_{\text{obs}} = K_1 k_{+2} ([\text{ATP}]/(1 + [\text{ADP}]/K_{\text{AD}})) \quad (3)$$

where k_{obs} is the observed rate constant for the ATP-induced dissociation of acto-S1, $K_1 k_{+2}$ is the second-order rate constant for ATP binding to acto-S1, and K_{AD} is the equilibrium dissociation constant for the binding of ADP to acto-S1. The equation $k_{\text{rel}} = k_{\text{obs}}/k_o$ was used to determine the relative rate constant (k_{rel}) shown in Fig. 5, where k_o is the value of the measured rate constant k_{obs} when $[\text{ADP}] = 0$.

Homology modeling

3D homology models were generated for the *Drosophila* IFI and EMB myosin motor domain and the exon 9 chimeric molecules using the SWISS-MODEL⁴¹ automatic comparative protein modeling server as described previously.³⁹ The primary sequences of the *Drosophila* IFI and EMB isoform were pairwise aligned with the sequence of four scallop myosin structures as templates (ExPDB 1kk8, 1qvi, 1s5g, and 1sr6) using the CLUSTALW alignment protocol. The alignments were submitted to the alignment interface of SWISS-MODEL and the generated models were validated using WHAT CHECK.⁴² Since the template coordinates cannot be used to model regions of insertions or deletions in the target-template alignment, an ensemble of fragments compatible with the neighboring stems was constructed using constraint space programming.⁴¹ In cases where constraint space programming does not give a satisfying solution and for loops above 10 residues, a loop library derived from experimental structures was searched to find compatible loop fragments. Both *Drosophila* IFI and EMB



Scheme 1. The interaction of S1 with actin, ATP, and ADP. M, A, T, and D symbolize S1, actin, ATP, and ADP, respectively.

myosin head sequences showed significant sequence identity with various other myosin superfamily members. A sequence identity of 60% ($\pm 1\%$) was found when IFI and EMB myosin head sequences were aligned with class II scallop myosin, thus enabling us to build well-resolved homology models.³⁹ Crystal structures of the various states of scallop myosin during the cross-bridge cycle are available, and these were chosen to generate 3D homology models of the IFI and EMB myosin heads as well as models of the chimeras obtained after swapping the exon 9-encoded region (IFI-9b and EMB-9a). Three of the scallop myosin structures used as templates contain a nucleotide in the binding pocket and they represent various conformational states of myosin during the cross-bridge cycle: the postpower stroke state contains ADP-BeF_x (ExPDB 1kk8), the prepower stroke state contains ADP-VO₄ (ExPDB 1qvi), and a novel conformation contains partially bound ADP-SO₄ (ExPDB 1s5g). The other scallop myosin structure does not have a nucleotide in the binding pocket (ExPDB 1sr6) and represents the near-rigor state of myosin. The generated models have Ramachandran Z scores of -0.469 (± 0.104) and average packing Z scores of -1.075 (± 0.075), which are within the expected range for well-refined structures. The overall topology of the models was similar to that of the scallop myosin II templates (average rmsd of the backbone is 0.17 ± 0.03 Å).

Acknowledgements

This work was supported by NIH grant GM32443 (to S.I.B.) and Wellcome Trust grant 070021 (to M.A.G.). We thank Martin Webb (National Institute for Medical Research, Mill Hill, London, UK) for the coumarin ATP/ADP used in this work and Anju Melkani for excellent technical support.

Supplementary Data

Supplementary data associated with this article can be found, in the online version, at [doi:10.1016/j.jmb.2009.04.036](https://doi.org/10.1016/j.jmb.2009.04.036)

References

- Richards, T. A. & Cavalier-Smith, T. (2005). Myosin domain evolution and the primary divergence of eukaryotes. *Nature*, **436**, 1113–1118.
- Foth, B. J., Goedecke, M. C. & Soldati, D. (2006). New insights into myosin evolution and classification. *Proc. Natl. Acad. Sci. USA*, **103**, 3681–3686.
- George, E. L., Ober, M. B. & Emerson, C. P., Jr (1989). Functional domains of the *Drosophila melanogaster* muscle myosin heavy-chain gene are encoded by alternatively spliced exons. *Mol. Cell. Biol.* **9**, 2957–2974.
- Bernstein, S. I. & Milligan, R. A. (1997). Fine tuning a molecular motor: the location of alternative domains in the *Drosophila* myosin head. *J. Mol. Biol.* **271**, 1–6.
- Koppole, S., Smith, J. & Fischer, S. (2007). The structural coupling between ATPase activation and recovery stroke in the myosin II motor. *Structure*, **15**, 825–837.
- Holmes, K. C., Schroder, R. R., Sweeney, H. L. & Houdusse, A. (2004). The structure of the rigor complex and its implications for the power stroke. *Philos. Trans. R. Soc. London, Ser. B*, **359**, 1819–1828.
- Houdusse, A., Szent-Gyorgyi, A. G. & Cohen, C. (2000). Three conformational states of scallop myosin S1. *Proc. Natl. Acad. Sci. USA*, **97**, 11238–11243.
- Zhang, S. & Bernstein, S. I. (2001). Spatially and temporally regulated expression of myosin heavy chain alternative exons during *Drosophila* embryogenesis. *Mech. Dev.* **101**, 35–45.
- Kronert, W. A., Dambacher, C. M., Knowles, A. F., Swank, D. M. & Bernstein, S. I. (2008). Alternative relay domains of *Drosophila melanogaster* myosin differentially affect ATPase activity, in vitro motility, myofibril structure and muscle function. *J. Mol. Biol.* **379**, 443–456.
- Swank, D. M., Knowles, A. F., Kronert, W. A., Suggs, J. A., Morrill, G. E., Nikkhoy, M. *et al.* (2003). Variable N-terminal regions of muscle myosin heavy chain modulate ATPase rate and actin sliding velocity. *J. Biol. Chem.* **278**, 17475–17482.
- Clark, R. J., Nyitrai, M., Webb, M. R. & Geeves, M. A. (2003). Probing nucleotide dissociation from myosin in vitro using microgram quantities of myosin. *J. Muscle Res. Cell Motil.* **24**, 317–323.
- Miller, B. M., Nyitrai, M., Bernstein, S. I. & Geeves, M. A. (2003). Kinetic analysis of *Drosophila* muscle myosin isoforms suggests a novel mode of mechanochemical coupling. *J. Biol. Chem.* **278**, 50293–50300.
- Weiss, S., Chizhov, I. & Geeves, M. A. (2000). A flash photolysis fluorescence/light scattering apparatus for use with sub microgram quantities of muscle proteins. *J. Muscle Res. Cell Motil.* **21**, 423–432.
- Cope, M. W., J., I. & Kendrick-Jones, J. K. (1996). Conservation within the myosin motor domain: implications for structure and function. *Structure*, **4**, 969–987.
- Geeves, M. A. & Holmes, K. C. (2005). The molecular mechanism of muscle contraction. In *Advances in Protein Chemistry* (Squire, J. M. & Parry, D. A. D., eds), pp. 161–193, Academic Press, San Diego, CA.
- Fischer, S., Windshugel, B., Horak, D., Holmes, K. C. & Smith, J. C. (2005). Structural mechanism of the recovery stroke in the myosin molecular motor. *Proc. Natl. Acad. Sci. USA*, **102**, 6873–6878.
- Sterner, R. H. & Liebl, W. (2001). Thermophilic adaptation of proteins. *Crit. Rev. Biochem. Mol. Biol.* **36**, 39–106.
- Margossian, S. S. & Lowey, S. (1973). Substructure of the myosin molecule. IV. Interactions of myosin and its subfragments with adenosine triphosphate and F-actin. *J. Mol. Biol.* **74**, 313–330.
- Shih, W. M. & Spudich, J. A. (2001). The myosin relay helix to converter interface remains intact throughout the actomyosin ATPase cycle. *J. Biol. Chem.* **276**, 19491–19494.
- Yang, C., Ramanath, S., Kronert, W. A., Bernstein, S. I., Maughan, D. W. & Swank, D. M. (2008). Alternative versions of the myosin relay domain differentially respond to load to influence *Drosophila* muscle kinetics. *Biophys. J.* **95**, 5228–5237.
- Swank, D. M., Knowles, A. F., Suggs, J. A., Sarsoza, F., Lee, A., Maughan, D. W. & Bernstein, S. I. (2002). The myosin converter domain modulates muscle performance. *Nat. Cell Biol.* **4**, 312.
- Holmes, K. C., Angert, I., Jon Kull, F., Jahn, W. & Schroder, R. R. (2003). Electron cryo-microscopy

- shows how strong binding of myosin to actin releases nucleotide. *Nature*, **425**, 423–427.
23. Woehlke, G., Ruby, A. K., Hart, C. L., Ly, B., Hom-Booher, N. & Vale, R. D. (1997). Microtubule interaction site of the kinesin motor. *Cell*, **90**, 207–216.
 24. Menetrey, J., Bahloul, A., Wells, A. L., Yengo, C. M., Morris, C. A., Sweeney, H. L. & Houdusse, A. (2005). The structure of the myosin VI motor reveals the mechanism of directionality reversal. *Nature*, **435**, 779–785.
 25. Menetrey, J., Llinas, P., Mukherjee, M., Sweeney, H. L. & Houdusse, A. (2007). The structural basis for the large powerstroke of myosin VI. *Cell*, **131**, 300–308.
 26. Richard, P., Charron, P., Carrier, L., Ledeuil, C., Cheav, T., Pichereau, C. *et al.* (2003). Hypertrophic cardiomyopathy: distribution of disease genes, spectrum of mutations, and implications for a molecular diagnosis strategy. *Circulation*, **107**, 2227–2232.
 27. Richard, P., Isnard, R., Carrier, L., Dubourg, O., Donatien, Y., Mathieu, B. *et al.* (1999). Double heterozygosity for mutations in the beta-myosin heavy chain and in the cardiac myosin binding protein C genes in a family with hypertrophic cardiomyopathy. *J. Med. Genet.* **36**, 542–545.
 28. Gorham, J., Seidman, C., Seidman, J. C. (2006). *Genomics of Cardiovascular Development, Adaptation, and Remodeling*. NHLBI Program for Genomic Applications, Harvard Medical School. <http://www.cardiogenomics.org>
 29. Arad, M., Penas-Lado, M., Monserrat, L., Maron, B. J., Sherrid, M., Ho, C. Y. *et al.* (2005). Gene mutations in apical hypertrophic cardiomyopathy. *Circulation*, **112**, 2805–2811.
 30. Moolman-Smook, J. C., De Lange, W. J., Bruwer, E. C., Brink, P. A. & Corfield, V. A. (1999). The origins of hypertrophic cardiomyopathy-causing mutations in two South African subpopulations: a unique profile of both independent and founder events. *Am. J. Hum. Genet.* **65**, 1308–1320.
 31. Mohiddin, S. A., Begley, D. A., McLam, E., Cardoso, J. P., Winkler, J. B., Sellers, J. R. & Fananapazir, L. (2003). Utility of genetic screening in hypertrophic cardiomyopathy: prevalence and significance of novel and double (homozygous and heterozygous) beta-myosin mutations. *Genet. Test.* **7**, 21–27.
 32. Song, L., Zou, Y., Wang, J., Wang, Z., Zhen, Y., Lou, K. *et al.* (2005). Mutations profile in Chinese patients with hypertrophic cardiomyopathy. *Clin. Chim. Acta*, **351**, 209–216.
 33. Van Driest, S. L., Jaeger, M. A., Ommen, S. R., Will, M. L., Gersh, B. J., Tajik, A. J. & Ackerman, M. J. (2004). Comprehensive analysis of the beta-myosin heavy chain gene in 389 unrelated patients with hypertrophic cardiomyopathy. *J. Am. Coll. Cardiol.* **44**, 602–610.
 34. Anan, R., Greve, G., Thierfelder, L., Watkins, H., McKenna, W. J., Solomon, S. *et al.* (1994). Prognostic implications of novel beta cardiac myosin heavy chain gene mutations that cause familial hypertrophic cardiomyopathy. *J. Clin. Invest.* **93**, 280–285.
 35. Nanni, L., Pieroni, M., Chimenti, C., Simionati, B., Zimbello, R., Maseri, A. *et al.* (2003). Hypertrophic cardiomyopathy: two homozygous cases with “typical” hypertrophic cardiomyopathy and three new mutations in cases with progression to dilated cardiomyopathy. *Biochem. Biophys. Res. Commun.* **309**, 391–398.
 36. Cammarato, A., Dambacher, C. M., Knowles, A. F., Kronert, W. A., Bodmer, R., Ocorr, K. & Bernstein, S. I. (2007). Myosin transducer mutations differentially affect motor function, myofibril structure, and the performance of skeletal and cardiac muscles. *Mol. Biol. Cell*, **19**, 553–562.
 37. Silva, R., Sparrow, J. & Geeves, M. (2003). Isolation and kinetic characterisation of myosin and myosin S1 from the *Drosophila* indirect flight muscles. *J. Muscle Res. Cell Motil.* **24**, 489–498.
 38. Pardee, J. D. & Spudis, J. A. (1982). Purification of muscle actin. *Methods Enzymol.* **85 Pt B**, 164–181.
 39. Miller, B. M., Bloemink, M. J., Nyitrai, M., Bernstein, S. I. & Geeves, M. A. (2007). A variable domain near the ATP-binding site in *Drosophila* muscle myosin is part of the communication pathway between the nucleotide and actin-binding sites. *J. Mol. Biol.* **368**, 1051–1066.
 40. Webb, M. R. & Corrie, J. E. T. (2001). Fluorescent coumarin-labeled nucleotides to measure ADP release from actomyosin. *Biophys. J.* **81**, 1562–1569.
 41. Schwede, T., Kopp, J., Guex, N. & Peitsch, M. C. (2003). SWISS-MODEL: an automated protein homology-modeling server. *Nucleic Acids Res.* **31**, 3381–3385.
 42. Hooft, R. W. W., Vriend, G., Sander, C. & Abola, E. E. (1996). Errors in protein structures. *Nature*, **381**, 272.